Underwater Mobile Manipulation

A Soft Arm on a Benthic Legged Robot

By Jiaqi Liu, Saverio Iacoponi, Cecilia Laschi, Li Wen, and Marcello Calisti

Robotic systems that can explore the sea floor, collect marine samples, gather shallow water refuse, and perform other underwater tasks are interesting and important in several fields, from biology and ecology to off-shore industry. In this article, we present a robotic platform that is, to our knowledge, the first to combine benthic legged locomotion and soft continuum manipulation to perform real-world underwater mission-like experiments. We experimentally exploit inverse kinematics for spatial manipulation in a laboratory environment and then examine the robot's workspace extensibility, force, energy consumption, and grasping ability in different undersea scenarios.

A six-legged benthic robotic platform, the Seabed Interaction Legged Vehicle for Exploration and Research, Version 2 (SILVER2), acted as the soft manipulation system's mobile base. The results show that the soft manipulator's workspace can be significantly extended by adding a benthic legged robot as a mobile base. We show that this system can precisely and effectively approach objects and perform dexterous grasping tasks, including retrieving objects from deep apertures in overhang environments. This robotic system has the potential to scale up to make shallow water collection tasks safer and more efficient.

Digital Object Identifier 10.1109/MRA.2020.3024001
Date of current version: 7 October 2020

Deep Sea Challenges

Oceanic exploration is considered a frontier for understanding our planet and its changes, searching for new resources, sustaining populations, and even discovering novel medical therapies. At present, however, less than five percent of our oceans has been thoroughly explored. Oceanic exploration can be costly, dangerous, impractical, and logistically challenging [1]. During recent years, demand for robots capable of underwater exploration and manipulation has grown immensely and is expected to continue to increase during the coming decades. Researchers and marine enterprises require reliable and low-cost underwater robots to unveil the

1070-9932/20©2020IEEE

mysteries of the oceans and boost the so-called blue economy [2].

Underwater Mobile Manipulation

The two main categories of underwater robots are remotely operated vehicles (ROVs) and autonomous underwater vehicles (AUVs). ROVs are usually employed for interaction tasks, with manipulators mounted to the main frame to facilitate remote operation. This subcategory of ROVs, known as the *underwater vehicle–manipulator system* (*UVMS*), is essentially a mobile robot that performs so-called floating manipulation [3]. This complex task requires a shared controller between the operator and the vehicle: high-level requests from the operator to hold a position or interact with an object are transformed into an actuator command for a vehicle's thrust and manipulation systems. But optimal UVMS performance is challenged by the mathematical complexity of the robotic system, imprecise modeling of thruster dynamics, limited sensing capabilities, and harsh and rapidly changing environmental conditions [4]. Researchers have devoted considerable attention to improving the floating manipulation and control of UVMSs during recent years. In simulations [5], undisturbed swimming pools [6], and pools with a current-like disturbance, researchers have demonstrated control capabilities that have errors on the order of a few centimeters. Despite these promising results, most ROVs still need to rest on the seafloor for stability when manipulation is required [7].

Another class of underwater vehicles, called *benthic crawlers*, facilitates interaction with underwater structures, without increasing control complexity, by maneuvering on the seabed via tracks and wheels. They are routinely used for heavy work duties, shallow water investigations, and long-term monitoring despite the fact that they are limited to substrates where tracks and wheels can be used [8]. A few recent examples of legged benthic robots, developed to withstand high currents [9], [10], move across uneven terrain [11], operate without disturbing the environment [12], and work in shallow water, promise to integrate the advantages of benthic crawlers with the dexterity of legged robots. With legged systems, researchers envision the possibility of precise and swift seabed interaction without the added complexity of controlling underwater stability. In addition, improved visibility can be achieved by the benthic crawler's legs (compared to propellers) while performing locomotion on sandy substrates. The actions of propellers often raise sand particles, which can reduce visibility; in our case, precise and slow positioning of the legs could prevent this from happening.

Underwater Soft Manipulation

A robot's manipulator system is another essential component to facilitate optimal underwater performance. Traditional underwater hydraulic robotic arms and grippers are designed for missions with heavy payloads and high levels of force [13]. These metal components are poorly suited for grasping fragile and squishable objects. Additionally, a massive metal arm has a large inertia, making underwater mobility challenging for a robot in unsteady conditions. Soft materials and bioinspired structures have immense potential to integrate flexible, lightweight elements into manipulators to reduce the mass and decrease the chance of damaging fragile objects. For example, previous work on an octopus-inspired soft arm achieved tethered motion under water [14], and a dexterous subsea hand [15] has been tested as a gripper. More recently, studies on soft robotic manipulation have begun to focus on underwater applications [16], [17], a silicone–rubber gripper [18], a modular soft robotic wrist [19], a dexterous glove-based soft arm [20], and a jamming gripper [21] have all been tested to grasp delicate underwater organisms at shallow-to-deep-sea depths. Thus, a soft manipulator—a combination of a soft arm and a gripper—may be a practical tool for real-world mobile underwater manipulation.

In this article, we investigate, for the first time, an integrated mobile benthic platform and a soft manipulator (Figure 1). For the benthic platform, we use SILVER2 [22], a six-legged, crab-inspired robot developed for exploration and environmental monitoring. For the manipulator, we use a soft device with a four-fingered soft gripper that can move in a 3D domain and perform delicate grasping. We experimentally employ spatial manipulation with inverse kinematics specifically for collecting tasks in a natural underwater environment. Both systems have been separately designed and optimized to serve as general-purpose underwater robots with locomotion and manipulation capabilities, respectively. SILVER2 was designed to have payload capacity for instruments, sensors, and a robot arm. The soft arm was planned to be mounted on underwater vehicles in a general way, and it fits SILVER2, as well. The possibility of integrating these two robots offers unique opportunities for testing each system and showing the benthic operation of robots. We hypothesize that fusing a benthic platform and a soft manipulator will combine the advantages of both innovative solutions for underwater operations.

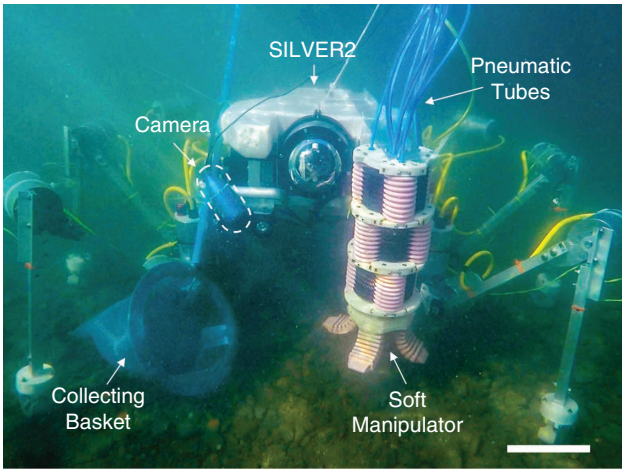

Figure 1. SILVER2 and its soft manipulator collecting a plastic bottle from the seabed. Scale bar: 15 cm.

Experimental Platform

The SILVER2 platform has several promising features, including efficient aquatic walking ability, underwater self-stabilization, and functional payload capacity for supporting the soft arm. SILVER2 was previously introduced in [12] and is briefly reviewed here for the necessary context. It consists of a central body with six articulated legs. The body is an open frame structure composed of two vertical plates connected by horizontal beams. Two main canisters (pressurized cylinders) mounted on the frame contain the battery pack (with a 300-Wh lithium polymer battery) and all the electronic components of the system (excluding cameras and actuators), respectively. A third auxiliary canister, with a transparent dome and two cameras, is attached to the front. The cameras are fixed to an actuated gimbal with two degrees of freedom (DoF). Floating foam and weights are attached to the frame to balance the system and obtain a weak negative buoyancy. Extra weights can be added to achieve a desired wet weight, depending on the nature of the mission. In the present study, the wet weight of the robot, including the manipulator, was 4.4 kg.

Each leg is composed of two links and three actuators. The links are square aluminum bars, and each actuator is encapsulated in its own dedicated canister. The first actuator (the coxa motor) controls the yaw [q_1 in Figure 2(a) and (b)] of the leg compared to the main body and is fixed to the main frame. The second actuator (the femur motor) is mounted close to the first and attached to the shaft of the first through an aluminum connector. The second and third actuators (the tibia motor) move the two-leg segments on the vertical plane [with angles q_2 and q_3, as shown in Figure 2(c)]. The second segment is connected to the third actuator shaft through a torsional elastic joint that is tuned to achieve the behavior predicted by the underwater spring-loaded inverted pendulum (USLIP) model, as in previous multilegged implementations [11]. The elastic joint and the third actuator form the serial elastic actuator (SEA) of the leg [23].

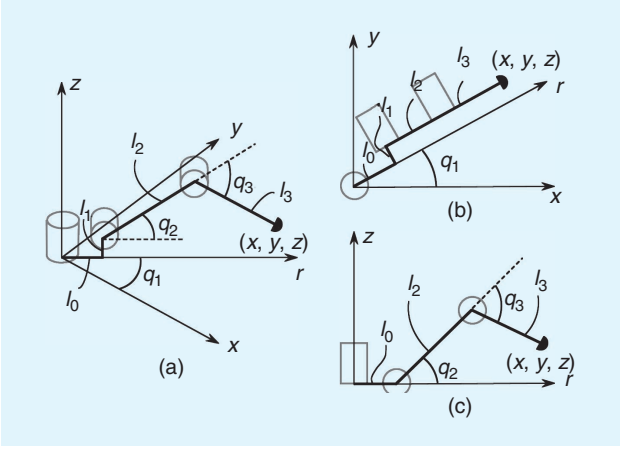

Figure 2. SILVER2's leg kinematics. (a) One leg's geometries, with a reference frame centered on the shaft of the coxa motor. All motors are represented as shadowed cylinders. Auxiliary views are reported in (b) and (c). Plane (r, z) in (c) is also called the *coxa plane*: its orientation around the z-axis is given by q_1, while the leg's position within the coxa plane is defined by angles q_2 and q_3.

SILVER2 is capable of static and dynamic locomotion. Static gaits are preprogrammed walking cycles for which the operator can choose the direction, speed, and other parameters. Dynamic locomotion is based on a hopping gait according to USLIP dynamics [24]. The operator can select key locomotion parameters on a computer, and self-stabilizing open-loop cycles ensure terrain negotiation. Due to the short distance required for the present analysis, only static walking gaits were employed. Each of the second segments of SILVER2's legs has a foot. A foot consists of an encapsulated piezoelectric disk and a hammer–hinge mechanism that compresses the piezoelectric component on contact with the ground, which sends a signal to the electronics canister. All canisters are connected with flexible underwater wires and penetrators.

A cable connects the platform to a floating buoy equipped with a Wi-Fi antenna to connect the operator and SILVER2. For all the present tests, a mechanical interface component was added to enable the addition of the soft arm. The arm was fixed at the top left of the structural frame. An additional underwater camera was mounted on the top right to provide visual feedback for the arm's operator.

SILVER2 Kinematics

For convenience, this section briefly summarizes SILVER2's kinematics and control; for further details, consult [12]. Using Figure 2(a)–(c) as a reference, the (x, y, z) position (see Figure 2 for the notation) of a SILVER2 leg is derived from direct kinematics:

$$\begin{cases} x = (l_0 + l_2\cos q_2 + l_3\cos(q_2 - q_3))\cos q_1 - l_1\cos q_1 \\ y = (l_0 + l_2\cos q_2 + l_3\cos(q_2 - q_3))\sin q_1 - l_1\sin q_1 \\ z = l_2\sin q_2 + l_3\sin(q_2 - q_3). \end{cases} \tag{1a}$$

Angles are retrieved by inverse kinematic equations:

$$\begin{cases} L = \sqrt{x^2 + y^2} \\ \beta = \operatorname{atan2}(y, x) \\ \gamma = \operatorname{atan2}(l_1, \sqrt{L^2 - l_1^2}) \\ r = L\cos(\gamma) - l_0 \\ m = \sqrt{r^2 + z^2} \\ q_1 = \beta - \gamma \\ q_2 = \operatorname{acos}\left(\dfrac{l_2^2 + m^2 - l_3^2}{2l_2 m}\right) + \operatorname{atan2}(z, r) \\ q_3 = \pi - \operatorname{acos}\left(\dfrac{l_2^2 - m^2 + l_3^2}{2l_2 l_3}\right), \end{cases} \tag{1b}$$

where l_0 and l_1 are the lengths of an L-shaped connecting element that links the coxa motor to the femur motor and the first segment of the leg, l_2. Eventually, link l_3 connects the knee of the leg to the foot. The DoF are the angular quantities

q_1, q_2, q_3 and L, β, γ, r, and m denotes simple auxiliary geometrical quantities that are easily derived from Figure 2(a)–(c). In Figure 2, r is an auxiliary axis that defines the plane of the second and third segments of a leg. Since this plane is defined by the coxa angle q_1, we refer to it as the *coxa plane*. The femur and tibia motors move the leg within the coxa plane (r, z), as shown in Figure 2(b). (The femur and tibia actually belong to a plane parallel to the coxa plane since segment l_1 produces a normal translation.)

By exploiting the relationships in (1a) and (1b), we implement a walking gait as linear trajectories (stance phases) followed by arcs (gliding phases) executed continuously by all the feet [see Figure 2(b)]. Feet trajectories are defined by two parameters: the elevation of the arc z_f and the linear distance on the ground d_f. Additional parameters can be selected to define different gaits, such as the elevation of the body from the ground, the width of the stance, the period required to execute the foot trajectory, the phase difference among leg activations, the duty factor of the walking motion, and the walking direction [12].

Soft Manipulator Kinematics

The soft manipulator is designed and fabricated for underwater grasping; its structure is shown in Figure 3. It primarily consists of three soft actuator modules and one soft gripper as the end effector and also has 10 pneumatic chambers there are three bending segments, and each has three chambers. The end effector four-fingered soft gripper is actuated by a single air inlet. The soft actuator modules and the soft gripper are modularly assembled by 3D-printed connectors and universal pneumatic joints. The soft manipulator is 435 mm in length (the soft arm is 310 mm, and the gripper is 125 mm) and 48 mm in diameter, with a total mass of 2,050 g in the air (210 g in water).

The inverse kinematics of soft continuum robots have attracted researchers' attention for a long time [25]–[27]. Here, we propose a rapid inverse solution based on the opposing actuation pattern [28]. We positioned the second soft actuator module to be a mirror image of the first segment. This optimized design simplifies the inverse kinematics modeling: by actuating opposite chambers in the first two segments, the segments generate the same curvature but in opposite directions, thus forming a sigmoidal "S" shape [Figure 3(a)]. Because of this structural design, the attitudes of the two bending segments are directly related. As a result, solving the inverse kinematics of a soft manipulator with opposing bending curvature requires computing only geometric functions when modeling the whole manipulator, so less computation time and fewer hardware resources are necessary. This actuation coupling reduces the modeling complexity of the soft manipulator.

When solving the inverse kinematics, we resolve the transformation from the given end effector coordinate $\{x_3, y_3, z_3, \theta_3, \varphi_3\}$ to chamber length $\{l_{ij}\}$, then to chamber pressure $\{p_{ij}\}$, where the transformation is from the task space to the joint space, and, finally, to the actuation space. More specifically, $\{p_{ij}\}$ represents the pressure within the chambers, and $\{l_{ij}\}$ indicates the chamber lengths, where, for p_{ij} and l_{ij}, the indexes $i = 1, 2, 3$ and $j = 1, 2, 3$ refer to the ith segment and the jth chamber. In addition, the initial length of the chambers $\{l_{ij\,\mathrm{int}}\}$ and constant parameter d could be measured before initiating actuation.

The constraints of our kinematics modeling were

$$\begin{cases} \theta_1 = \theta_2 \\ \varphi_1 = \varphi_2 + \pi \\ r_1 = r_2 \\ l_{1i} = l_{2i}\,(i = 1, 2, 3). \end{cases} \tag{1c}$$

As discussed previously, the manipulator has five DoF in coordinate space $\{x_3, y_3, z_3, \theta_3, \varphi_3\}$ and six independent chambers $\{l_{11}(l_{21}), l_{12}(l_{22}), l_{13}(l_{23})$ and $l_{31}, l_{32}, l_{33}\}$. To obtain the chamber lengths (six outputs) from the coordinates (five inputs), we implement another constraint condition for the inverse kinematics: at most, two chambers in the third segment are actuated at the same time, and at least one chamber in the third segment remains at its initial length.

With this constraint, the first step of this approach is determining which chamber of the third segment should not be actuated. Based on the geometric relationship shown in Figure 3(c) and (d), we developed an equation that represents the initial lengths regarding the arc parameters $\{r_3, \varphi_3, \theta_3\}$:

$$\begin{cases} l_{31\,\mathrm{int}} = \theta_3 \cdot r_{31} = \theta_3 \cdot (r_3 - d\sin\varphi_3), \\ \qquad \text{if} \dfrac{\pi}{6} \leqslant \varphi_3 < \dfrac{5\pi}{6} \\ l_{32\,\mathrm{int}} = \theta_3 \cdot r_{32} = \theta_3 \cdot \left[r_3 + d\cos\left(\varphi_3 - \dfrac{\pi}{6}\right)\right], \\ \qquad \text{if} \dfrac{5\pi}{6} \leqslant \varphi_3 < \dfrac{3\pi}{2} \\ l_{33\,\mathrm{int}} = \theta_3 \cdot r_{33} = \theta_3 \cdot \left[r_3 - d\cos\left(\varphi_3 + \dfrac{\pi}{6}\right)\right], \\ \qquad \text{if} \dfrac{3\pi}{2} \leqslant \varphi_3 < 2\pi \text{ or } 0 \leqslant \varphi_3 < \dfrac{\pi}{6}. \end{cases} \tag{1d}$$

By combining the given end effector coordinate $\{x_3, y_3, z_3, \theta_3, \varphi_3\}$ and (1d), we can obtain the value of r_3 and θ_3. Then, based on the geometric relationship shown in Figure 3(a), we developed another equation from the given coordinates:

$$\begin{cases} x_1 = \dfrac{x_3 - r_3(1 - \cos\theta_3)\cos\varphi_3}{2} = r_1(1 - \cos\theta_1)\cos\varphi_1 \\ y_1 = \dfrac{y_3 - r_3(1 - \cos\theta_3)\sin\varphi_3}{2} = r_1(1 - \cos\theta_1)\sin\varphi_1 \\ z_1 = \dfrac{z_3 - r_3\sin\theta_3}{2} = r_1\sin\theta_1. \end{cases} \tag{1e}$$

In (1e), only r_1, φ_1, and θ_1 are unknown. Combining (1d) and (1e) enables r_1, φ_1, and θ_1 to be analytically solved. Next, the calculated arc parameters $\{r_i, \varphi_i, \theta_i\}$ provide all the chamber parameters $\{l_{i1}, l_{i2}, l_{i3}\}$:

$$\begin{cases} l_{i1} = \theta_i \cdot (r_i - d\sin\varphi_i) \\ l_{i2} = \theta_i \cdot \left[r_i + d\cos\left(\varphi_i - \frac{\pi}{6}\right) \right] \\ l_{i3} = \theta_i \cdot \left[r_i - d\cos\left(\varphi_i + \frac{\pi}{6}\right) \right]. \end{cases} \tag{1f}$$

Thus, we obtained a specific inverse transformation from $\{x_3, y_3, z_3, \theta_3, \varphi_3\}$ to $\{l_{11}(l_{21}), l_{12}(l_{22}), l_{13}(l_{23}), l_{31}, l_{32}, l_{33}\}$. Adding a calibrated pressure length relationship [Figure 3(e)] enables us to calculate the driving pressure $\{p_{i1}, p_{i2}, p_{i3}\}$ from the chamber length $\{l_{11}(l_{21}), l_{12}(l_{22}), l_{13}(l_{23}), l_{31}, l_{32}, l_{33}\}$ to complete the model-based control.

Considering the influence of the rigid interface and buoyancy in the underwater environment, laboratory tests were carried out to compensate for the angle loss by adding a pneumatic pressure offset for each chamber to ensure that the opposite-bending S shape is maintained. In the calibration process, we use a parameter a to adjust the air pressure in the bending segments,

$$p_{1j} = a \cdot p_{2j} + b, \tag{1g}$$

where p_{1j} is the pressure of the jth chamber in segment 1 and p_{2j} is the pressure of the jth chamber in segment 2. This equation is fitted with the experimental calibration. The experiment suggests, that when $a = 1.02$ and $b = -0.89$ (linear fitting $R^2 = 0.9996$), (1g) works for the pneumatics actuation. As a result, the first and second segments of the soft manipulator achieve the expected orientation, i.e., the S-shape bend.

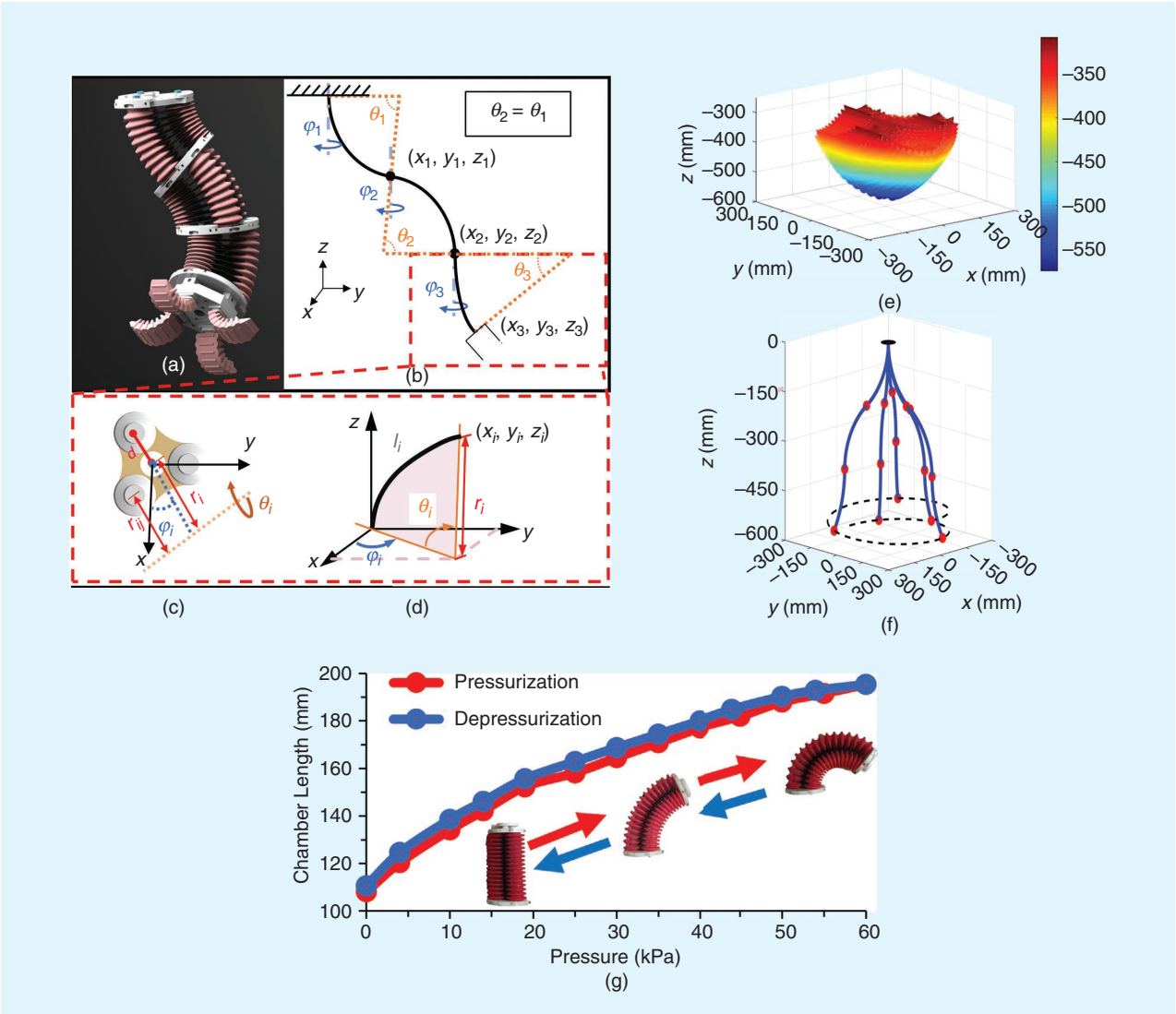

Figure 3. (a) A digital rendering of the soft manipulator. (b) A schema of the soft manipulator. (c) The geometric schematic of the bending segment of the constant-curvature soft manipulator. (d) The geometric functions in a bending segment, where φ_i is the deflection angle around the z-axis, θ_i is the curvature angle around the y-axis, and r_i is the curvature radius. (e) The simulated workspace of the soft manipulator. (f) The programmed trajectory paths based on the inverse kinematics method. Dashed lines indicate the helical-shaped trajectory, red dots denote the connection between chambers, and blue curves represent the time histories of soft arm movements during the tracking process. (g) The chamber lengths of the bending segments as a hysteretic function of the actuation pressure (0–60 kPa) in pressurization (red) and depressurization (blue).

The simulated workspace of the manipulator is displayed in Figure 3(f). The result shows that the manipulator can operate within a 3D space with a length of 500 mm, a width of 520 mm, and a height of 304 mm. The soft manipulator is actuated and controlled via the multichannel pneumatic control system presented in Figure 4. This system generates a separate pressure for all 10 pneumatic chambers, according to the inverse kinematic model. This system was offboarded and above water during all tests. Pneumatic tubes connect the system and the soft manipulator.

Experimental Protocols

We experimentally verified our system through a bottom-up approach that ended with mission-like trials. Protocols from A to C tested specific capabilities—the manipulator's force and precision—that could be compared with state-of-the-art results from traditional underwater robots. We further confirmed the system's effectiveness through two additional protocols, D and E, which aimed to 1) collect varied and fragile objects from the seabed and 2) manipulate objects in confined spaces, respectively. All experiments were performed in real shallow water mission conditions in the Tyrrhenian Sea, on the seabed at a specific depth of roughly 1.2 m, and all tests were repeated at least five times.

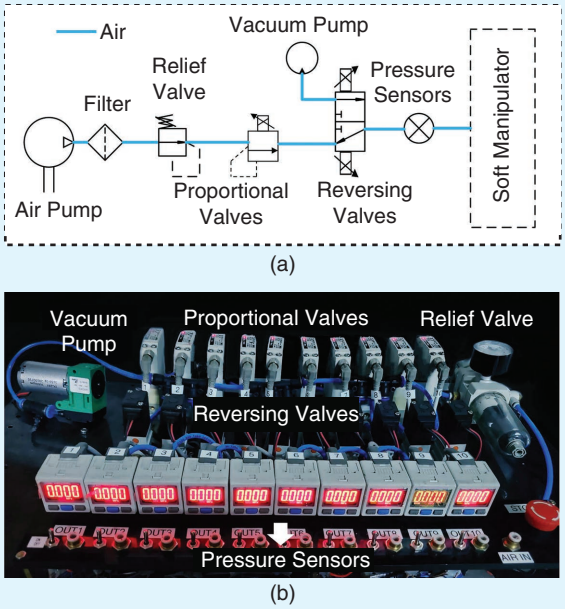

Figure 4. The multichannel pneumatic control system for the soft manipulator. (a) The framework of the system. (b) The hardware of the system, which contains a vacuum pump, 10 proportional valves, and 10 air pressure sensors.

Force Protocol

The first protocol aimed to measure the maximum pulling forces generated by SILVER2 and the soft arm system [Figure 5(a)]. Similar to conducting a vertical bollard pull, only static vertical pulling forces were measured in this study. For all tests, a hemispherical rubber handle was fixed close to the ground. The handle was attached to a load cell connected vertically to a plate. The plate was firmly anchored to the seafloor by a substantial amount of lead weight. The load cell was then connected to a force gauge (PCE_FM1000). For each test, the robot was manually positioned above the handle to ensure the vertical alignment of the arm and the correct gripper position. The test was interrupted when the maximum force value was reached or when the gripping failed. The highest force value was then recorded.

Since the robotic system can generate pulling force by either actuating the arm or extending the legs, we tested different configurations to highlight different capabilities. In configuration A, we measured the pulling force of the legs alone. The gripper was actuated to hold the handle, and then the legs were quickly extended (~200 mm/s) to generate a pulling force. In configuration B, we measured the maximum pulling force of the arm alone (~50 mm/s) while SILVER2 maintained a static position. In configuration C, we measured the interaction of the two main systems: the gripper grasped the handle, and the arm and the legs jointly performed a pulling action. In configuration D, we replicated the configuration A design but with the legs extending slowly (~50 mm/s). Finally, in configuration E, we connected SILVER2, without the arm, directly to the handle with a not-extensible wire. SILVER2's movements were monitored by an operator, and the arm movement was controlled with a camera mounted on the SILVER2 platform itself.

Workspace Protocol

The workspace protocol focused on measuring the enlargement of the manipulator workspace when it was mounted on SILVER2. In this protocol, SILVER2 and the manipulator grasped an object from a lower platform and released it in a target area at a height of 37 cm [Figure 5(b)]. The test consisted of two steps: first, SILVER2 was placed in front of the platform, and the soft manipulator grasped the object from the lower platform. Second, SILVER2 extended its legs without walking, and the manipulator executed several movements (~50 mm/s) to release the object at the target location. Specifically, the legs were elongated to gain approximately 20 cm in the vertical direction. Releasing the object on the target could be considered a success. The error was measured as the distance between the center of the object and that of the red, circular target. We also tested the performance of the soft manipulator without SILVER2. We placed the soft manipulator alone in the water tank and performed the same soft manipulator routine: moving an object from the bottom of the target area. Then, we measured the maximum height of the target area to which the soft manipulator could reach and release the object.

Mobile Pick-and-Place Protocol

This protocol [Figure 5(c)] was used to measure the performance of the whole system in a typical mobile manipulation

task. It enabled us to estimate the precision and effectiveness of the combined SILVER2–manipulator arm system. The test began with the arm grabbing the target object (a shell) and lifting it from the platform. Then, SILVER2 initiated a lateral walking gait (~150 mm/s) to reach the target zone, which was 2 m from the starting point. Once the target was within the workspace of the arm, the arm was actuated to place and release the object onto the target plate. The system's performance was evaluated by measuring the distance between the center of the object and that of the red circle for each trial. Releasing the object on the target plate could be considered a success.

Collecting Litter and Objects

With this protocol, we aimed to qualitatively assess the system's performance during a typical collection mission, either to perform seabed cleaning or retrieve a fragile biological specimen. The selected test objects were a hard silicone seashell; an eggshell, which simulated a fragile biological specimen; and three pieces of common trash found on the seabed: a plastic shopping bag, a plastic bottle (0.5 L), and a nylon fishing net (400 cm^2). Additionally, the net was tested in an entangled condition: a small rock (0.35 kg) was positioned directly in the middle of the net and placed onto the seabed.

The system's performance was evaluated by verifying whether the equipment was capable of completing the task. As is shown in Figure 6, the following steps were carried out and evaluated.

1) *Approaching the object*: The system should move roughly 2 m until the object is within the arm's workspace.
2) *Grasping the object*: The arm should retrieve the object from the seabed and firmly hold it against hydrodynamic disturbances.
3) *Releasing the object*: The gripper should be able to open its fingers to allow the object to fall freely.
4) *Collecting the object*: The target object should be stored in the side-mounted basket.

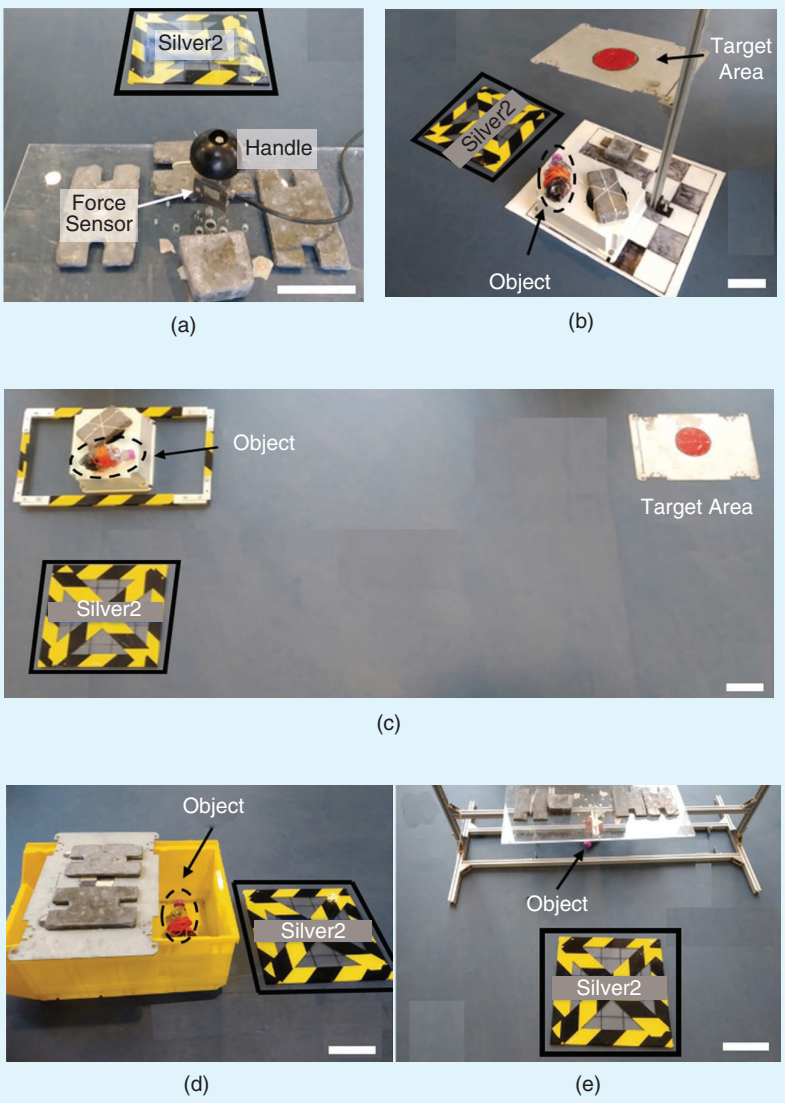

Figure 5. The experimental setup for different protocols conducted on the seafloor (depicted here as a dry environment for demonstration purposes). The (a) force protocol, (b) workspace protocol, (c) mobile pick-and-place protocol, and (d) and (e) confined environment protocol. The robot's initial position is represented by a labeled square. Scale bar: 15 cm.

Collecting Objects in Confined Spaces

In this protocol, we investigated whether our soft manipulator could retrieve objects from confined spaces and whether its light weight and compliance would be beneficial for underwater manipulation. Two tests were carried out to estimate the performance of the manipulator in a confined underwater environment. The first focused on collecting objects from a half-open box [Figure 5(d)]. The object and a real-time underwater camera (transmitting images via cables) were placed on the bottom of the box, and half of the box was then covered by a metal plate. The grasping task was executed in three steps:

1) SILVER2 was placed in front of the box, with the manipulator fully contracted, and it extended its legs to ensure that the manipulator was above the box.
2) SILVER2 lowered its legs, and the manipulator was able to reach into the box.

3) The manipulator grasped the object via the arm inverse kinematics model and took the article out of the box.

The performance during this test was evaluated by measuring the length of the opening area and verifying whether the system successfully grasped and collected the object.

The second test was carried out to collect objects from a simulated overhang environment [Figure 5(e)]. A transparent plate was fixed to a frame to create an overhang barrier, and the object was placed on the seabed. The grasping task consisted of two steps:

1) SILVER2 was placed in front of the frame, with the soft manipulator fully contracted.
2) The manipulator grasped the object using the soft arm (via the inverse kinematics model) and took the object from beneath the overhang.

The system's performance was evaluated by measuring the height of the plate and verifying whether the manipulator successfully grasped and collected the object.

Results

We conducted all experiments in realistic sea conditions, on both cloudy and sunny days without rain. The average depth of the robot for all tests was approximately 0.8 m; a pressure sensor placed beside one of the canisters recorded the actual depth of the body, which was above the seabed. A movie of the experiments is available in the supplementary video, which can be found on IEEE *Xplore*.

Force Experiments

Figure 7 conveys the results of the force tests. By evaluating different components separately and together, we were able to determine the relationship between the system's energy consumption and exerted force. The arm alone can exert a significant pulling force of roughly 16 N, on average (Figure 7b), using only the manipulator's pneumatic chambers. As a reaction to the pulling force, the legs required additional thrust to the motors to hold a static position, which led to a slightly increased energy consumption (electrical power from ~30 to ~36 W). This result can be directly compared to the power consumption of intervention AUVs (I-AUVs), which, like SILVER2, have onboard batteries. Experiments from 6-h operations of the Girona 500 show an overall energy consumption (during underwater transects and without actual arm interaction) of 1,026 Wh, with 570 Wh powering the thrusters and the remaining 456 Wh considered to be hotel energy. In the case of SILVER2 with an attached arm, operating (e.g., pulling an object) for 6 h will drain only 180 Wh of energy from the legs' motors, of which 35 Wh are required for SILVER2 to stand without operating. The advantages of benthic systems compared to hovering ones in terms of energy consumption are intuitively clear, and our reported results suggest possible energy savings of up to one order of magnitude.

Using the legs and the gripper [Figure 7(a)], we recorded a momentary but significant reduction in the average pulling force (8 N) and a corresponding increase in the power

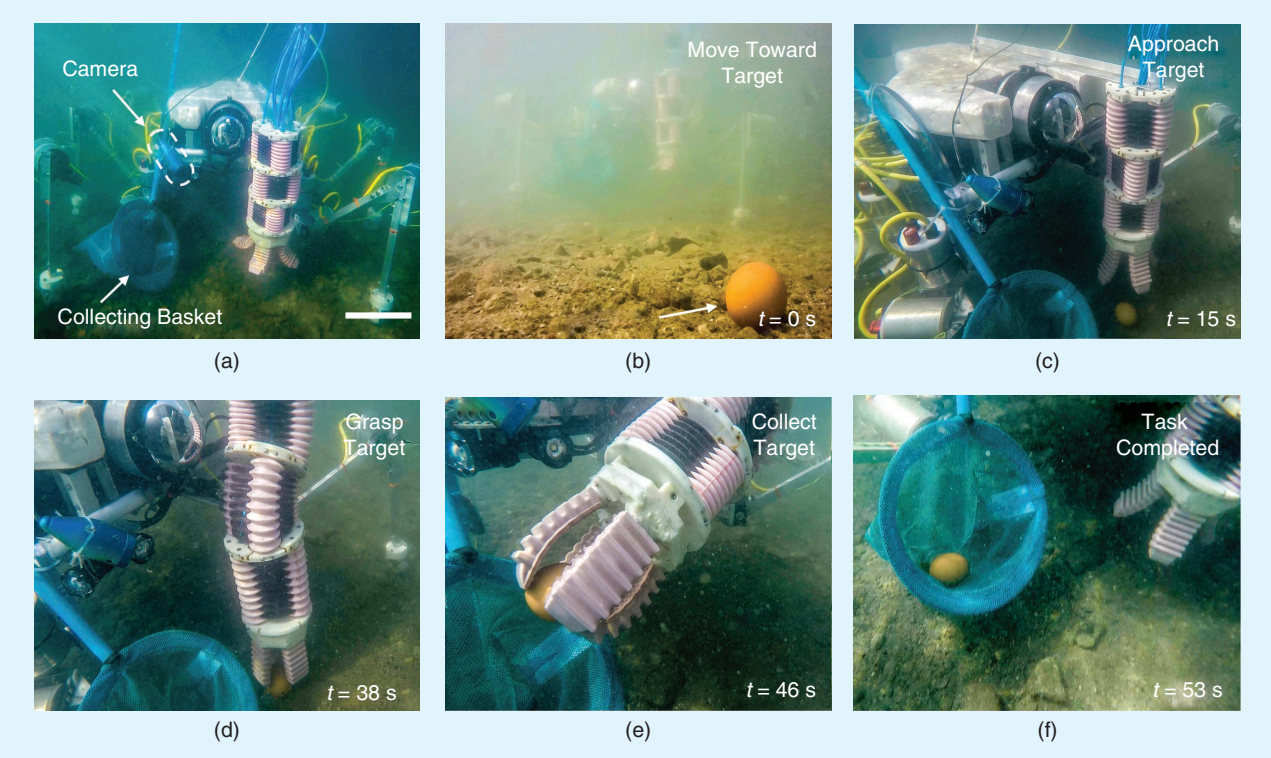

Figure 6. An example of fragile object collection. (a) The robot starts a few meters away from the object and (b) moves close enough so that the object (c) is within the arm's workspace. (d) The soft manipulator grasps the object via the inverse kinematics model and (e) moves it into (f) the onboard collection basket. Scale bar: 15 cm.

demand (roughly 132 W) for less than 1 s (0.8 s). The increase in the power consumption is consistent with a quick activation of the 12 motors to raise the body. The reduction in the pulling force is related to the opening of the soft gripper, which, subject to high acceleration, is not capable of conforming to the handle and establishing a firm grip. By using the arm and the legs together, we recorded a pulling force of 15 N [Figure 7(c)], similar to that achieved by the arm alone. By activating the arm first, the robot positioned the gripper in a suitable grasping position, so the subsequent activation of the legs fully exploited the potential of the gripper. By activating the legs very slowly and allowing the soft gripper to conform well to the handle [Figure 7(d)], we recorded an average force of approximately 18 N, confirming that slow acceleration enables a greater pulling force. In this case, the power consumption was reduced to a maximum value of roughly 96 W, even though the motion was maintained for 6 s, with an average power draw of 70 W [Figure 7(c)–(d)].

We also measured the power consumption of the soft manipulator (while grasping a shell with a size similar to the one that had been gripped on the seafloor) in the laboratory water tank. The system's power was recorded every 5 s by a power meter device (Zhejiang Shixin Electric). We calculated the average power consumption of the soft manipulator by recording data for 40 s. We also repeated each experimental scenario five times to acquire the mean value. The pneumatic control system's average power consumption was 25 ± 1 W. This result highlights a less-studied aspect of using a soft gripper for underwater grasping. Most existing research examines novel actuation methodologies, modeling, sensing, and fabrication methods. Our results indicate that the arm's speed and acceleration greatly influence the maximum grasping force. In addition to underwater operations, this finding may be particularly relevant for factories, warehouses, and other industrial settings that require quick handling.

Finally, the pulling force of the legs was measured by directly connecting a cable between the force sensor and

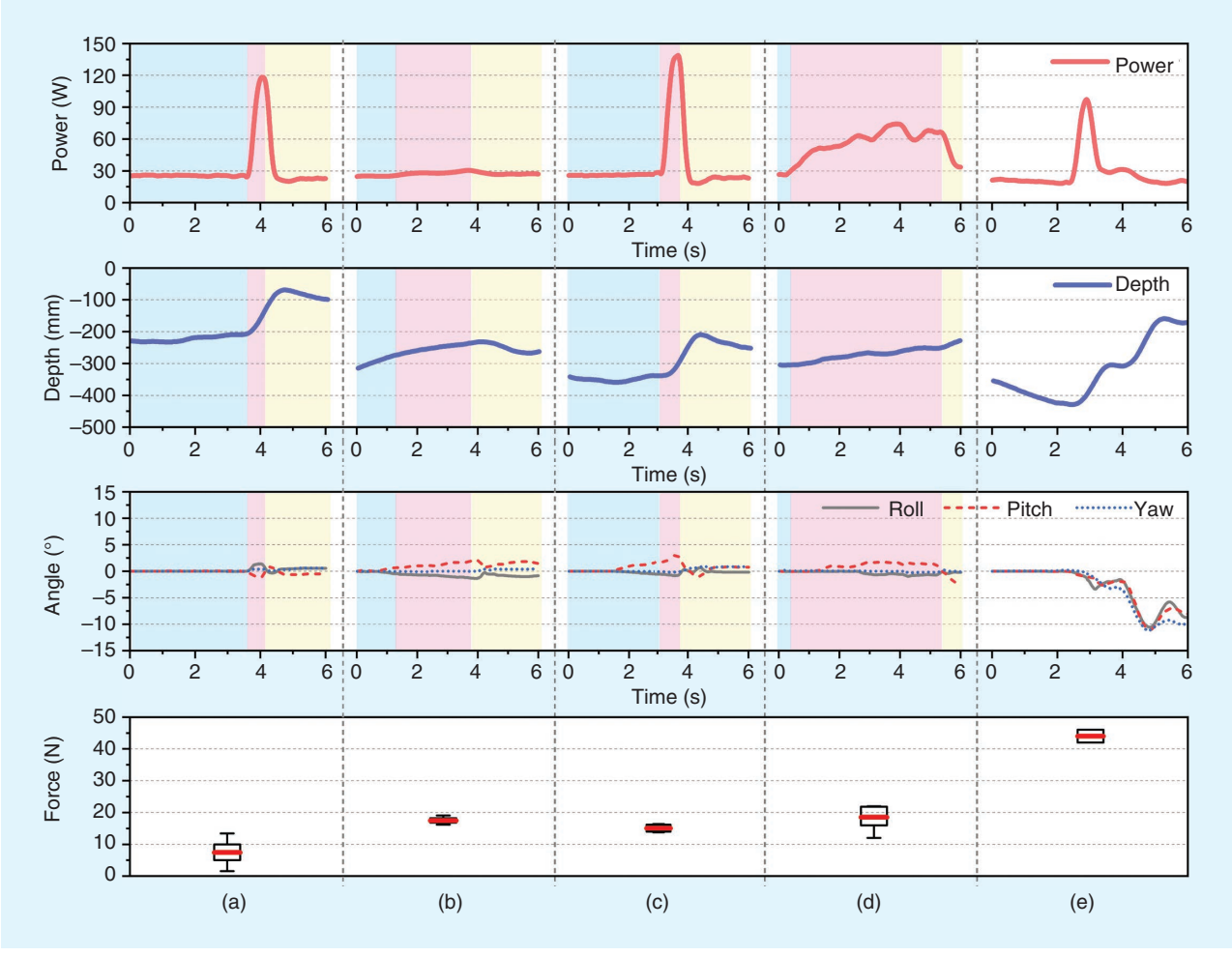

Figure 7. Typical results of the force protocol. The different experimental conditions are as follows: (a) the quick action of the legs and the gripper, (b) the arm movement alone, (c) the combined action of the legs and the arm, (d) the slow action of the legs and the gripper, and (e) the action of the legs alone (with a direct connection between the force sensor and the robot body). The power consumption, depth, tilt, and force of the robot are reported in the different rows of the figure. The force is given as a box plot of all collected data. The blue, pink, and yellow backgrounds represent the grasping, pulling, and releasing phases, respectively. Identical time windows are shown in the supplementary video, which can be found on IEEE *Xplore*.

the robot's body, without the involvement of the soft arm. Theoretically, the stall torque of the motors (3.8 N·m) exerted on a tibia length of approximately 0.35 m should result in a force of roughly 65 N for all the legs together. Actual measurements from experiments reported an average force of 44 N [Figure 7(e)]. The ratio between the measured and nominal forces is roughly 0.68, consistent with the expected losses from a servo motor system. For underwater vehicles, even with optimized blade designs, the efficiency would be reduced by the propeller efficiency to approximately 0.8 [29]. For an optimized AUV, the overall power efficiency for 7-N navigation is reported as 0.49. It is a reasonable expectation that direct transmission would slightly increase the force management and possibly exert a higher force on the environment. However, an ROV of comparable size to SILVER2 (the BlueROV2) demonstrates a nominal bollard vertical thrust of between 69 and 88 N. Without the necessary data for comparison, we can assume that the force and power consumption of SILVER2's legs alone fall between those of a small ROV and an I-AUV.

Workspace Protocol

An intrinsic advantage of mobile manipulation is that locomotion enables the manipulator workspace to be extended. Our protocol investigated vertical extensions first, as shown in Figure 8. In this case, the robot moved into a starting position and initiated a test. Compared with the soft manipulator working alone, we found that the vertical workspace of the soft manipulator increased 85% (from 20 to 37 cm) when it was integrated on SILVER2. With an average release error of 6.1 cm, the arm was capable of placing a portion of the shell in the red target area. Such an error is comparable to remotely controlled tests performed in the swimming pool [6], where a yellow tube was grasped during a collection task. In that example, precise positioning was not required if the mission was satisfactorily completed.

In previous work [5], simulations were performed for button-pushing and valve-turning tasks. The reported alignment error and the gripper and button modeling were slightly better than our present results. However, our results suggest that the button-pushing task could be accomplished, even with our average placement offset. In [30], the

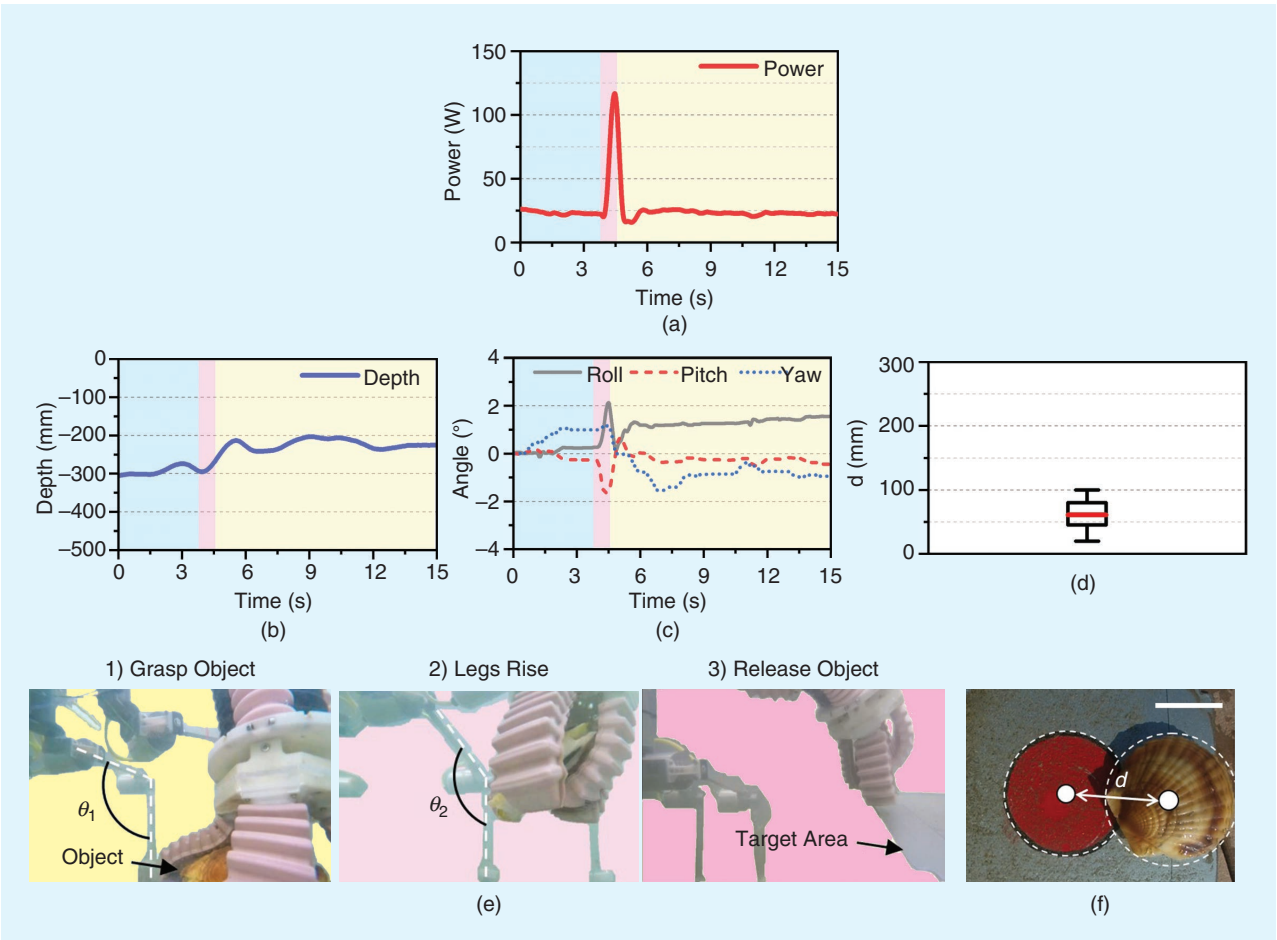

Figure 8. The results of the workspace protocol. The (a) power consumption, (b) SILVER2 depth, (c) body orientation and (d) placement error distances, representing all data collected during the experiments. (e) The yellow, pink, and purple backgrounds represent the grasping, standing, and releasing phases, respectively. (f) The object placement results. Scale bar: 5 cm.

authors report good results for the end effector positioning within an experimental tank and under a monodirectional simulated current. In that experiment, six cameras and Qualisys Track Manager (QTM) software were employed to evaluate the system's underwater pose. With an error of approximately 5.8 ± 3 cm, the experimental results demonstrate very accurate mobility and positioning. It is worth noting that the testing conditions presented in our experiments are poorly represented in the existing literature. All related work either accomplishes the target task through simulation or in controlled environments, such as a swimming pool or a tank. It is correctly reported in [30] that the position error via the QTM is difficult to obtain in field conditions, so the reported performance could vary significantly among different underwater environments.

Mobile Pick and Place

Compared to the results of the workspace protocol, the performance decreased in the horizontal workspace extension during an evaluation known as the *pick-and-place test*. In all attempts, the robot succeeded in bringing the target within the manipulator workspace (i.e., between the legs). During the release, we observed an average error of roughly 15.7 cm [Figure 9(d)]. This result enabled us to place the object in the desired area but not always within the red, circular target. We observed a primary reason for this decrease in the performance: disturbances on the benthic platform and the soft manipulator. SILVER2 does not have closed-loop station-keeping control, and we did not modify the position of the robot when unexpected currents significantly shifted it from the desired final location. With respect to the arm, although we never observed significant displacements, small vibrations may have impaired the release speed and increased the error.

It is worth mentioning that, in one trial, the shell was accidentally released during the walking phase from the starting point to the target area. This happened when we tested a faster walking speed (20 cm/s) and induced additional shaking in the arm. All the remaining trials were performed at an approximate walking speed of 5 cm/s. It is also worth remarking that all tests were conducted in conditions with relatively poor visibility that limited the details the underwater cameras could provide.

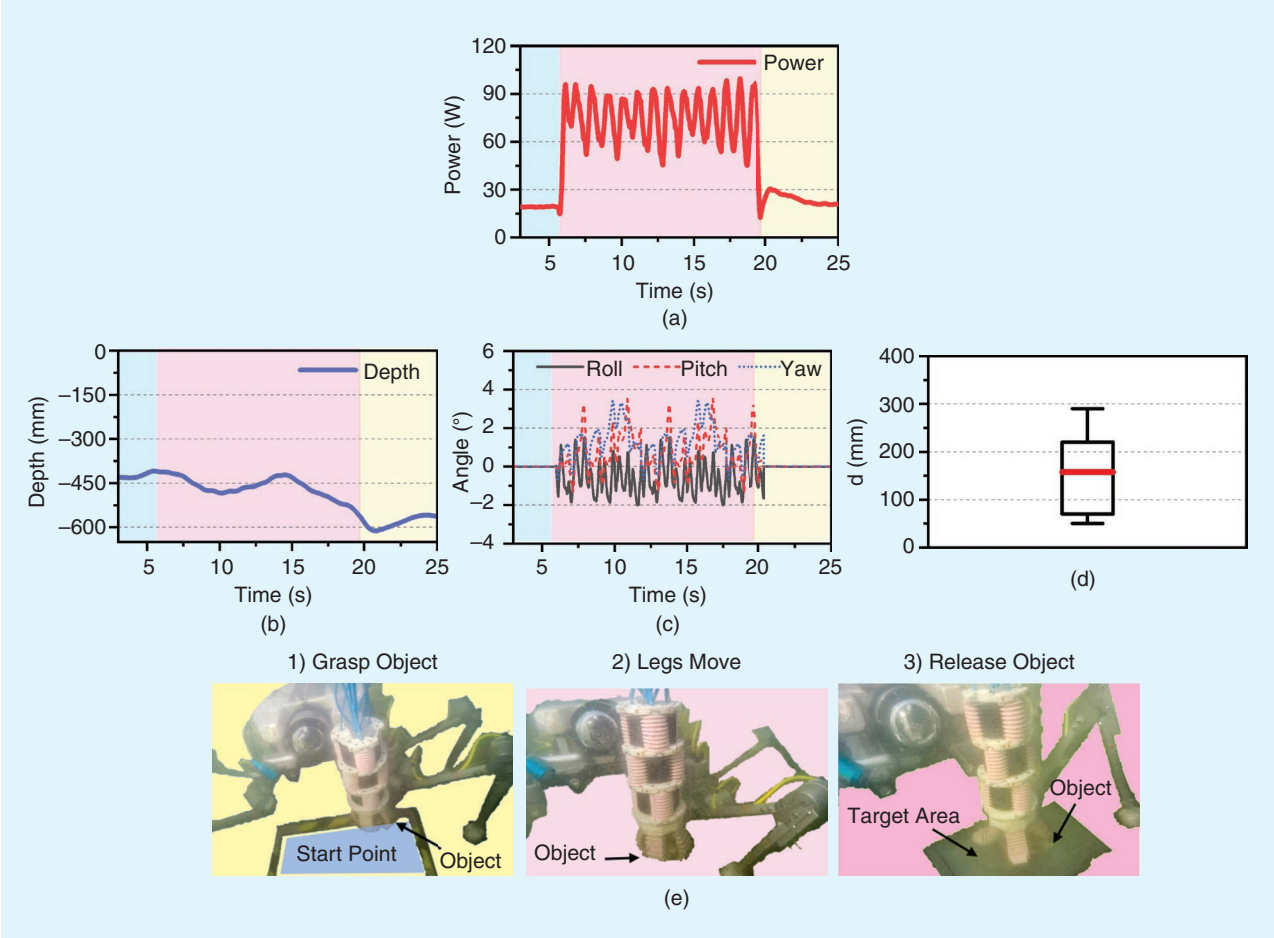

Figure 9. The results of the mobile pick and place. The (a) power consumption, (b) gripper depth, (c) body orientation, and (d) object placement offset distances, representing all the data collected during the experiments. (e) The yellow, pink, and purple backgrounds represent the grasping, standing, and releasing phases, respectively.

Litter and Fragile Object Collection

The results of this protocol are presented by object type. We qualitatively report (Figure 10) the binary success/failure of approaching, grasping, releasing, and collecting each object. The whole set of tested objects was successfully approached and grasped. The legs did not induce disturbances on the objects themselves, and the arm was capable of gripping and lifting the articles. Objects with a defined and solid shape (the plastic bottle, eggshell, and silicone seashell) were also positively released and collected. Objects that significantly deformed, namely, the plastic bag and the fishing net (protocols C and D), posed significant challenges for the gripper. Even though the objects were successfully released in some situations, in most trials, they got tangled in the gripper's fingers. The prevention of a proper release also impaired the collection into the onboard basket. In addition, we tested the system's disentangling force by placing the net below a large rock [Figure 10(f)]. In this case, the gripper was able to grasp the net, the legs helped disentangle the net by increasing the vertical workspace, and the motion eventually freed the net from the robot. In this case, the net was easily released by using a clear pinching grasp.

Collecting Objects in a Confined Space

This final protocol showcased the soft arm's ability to navigate and grasp in confined spaces. Given the rigid part of the manipulator's nominal size of 12 cm, we tested how well we were able to collect objects in a confined space. The minimum height of the overhang [Figure 11(a)] under which the robot succeeded in retrieving an object was 17 cm. The arm alone was sufficient for this task. During the box test [Figure 11(b)], the arm successfully negotiated a minimum 14-cm aperture. In this case, the legs controlled the vertical workspace to enable the arm to reach the most distant part of the box and helped move the object outside the box once the item was grasped. Without assistance from the legs, the arm released the shell after trying to force its way out of the confined environment.

Discussion

Our study investigated the interaction between a completely soft arm and a legged robot in a real-world underwater environment. In this section, we discuss the experimental results of the underwater manipulation, including both force and precision, and the application of those features for more complicated mission-like underwater experiments.

Simplifying the Soft Manipulator's Inverse Kinematics Problem

Solving higher-order nonlinear equations and training a practical kinematics model in oceanic environments remain challenging [28]. In this article, we proposed a simple and inverse kinematics solution for a soft manipulator—the opposite-bending S shape. The structure design offers advantages for the kinematic modeling of the manipulator since the attitudes of the two bending segments are directly related. As a result,

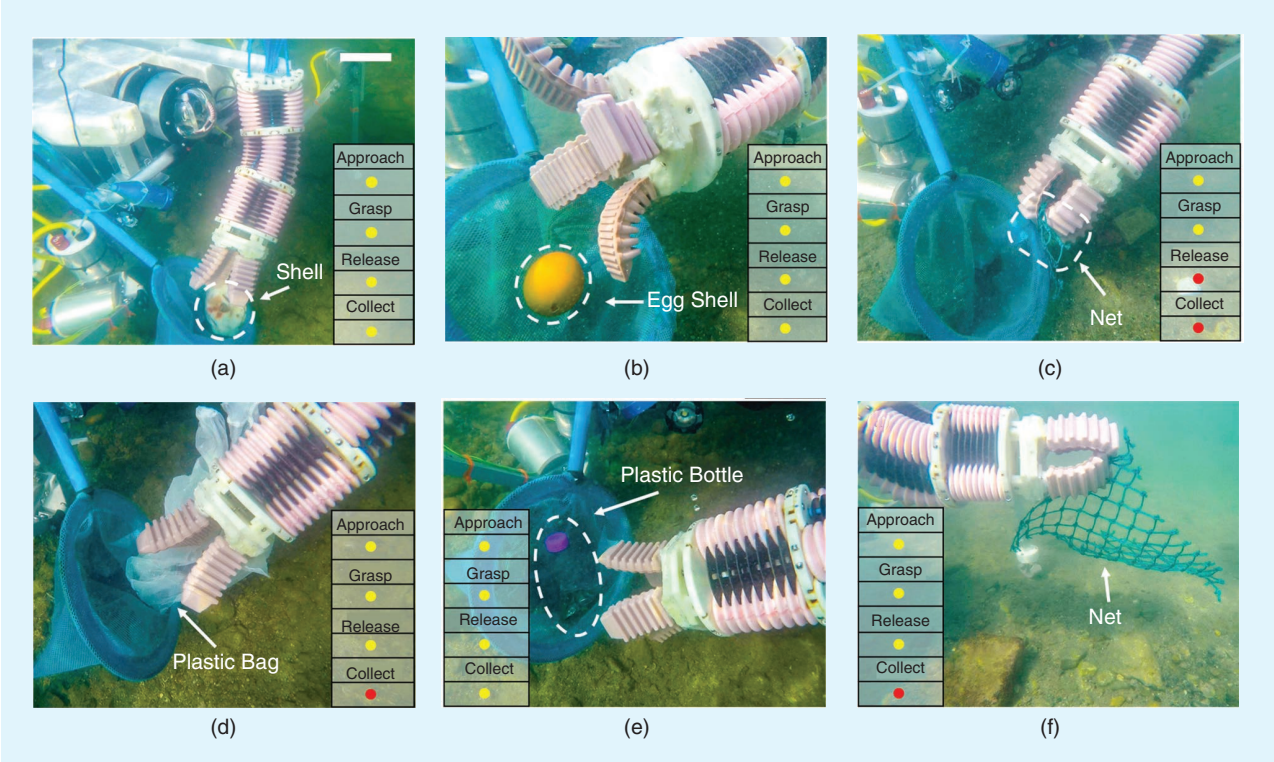

Figure 10. The results of the litter and fragile object collection protocol. The color of the marker in the table denotes a successful (yellow) or failed (red) step of each test. Different objects, such as (a) a seashell, (b) an eggshell, (c) and (f) a net, (d) a plastic bag, and (e) a plastic bottle, were used during the experiments. Scale bar: 5 cm.

solving the inverse kinematics of the soft manipulator with opposing curvature requires computing only geometric functions when modeling the whole manipulator. Compared with the previous opposite-bending-and-stretching structure modeling method [28] (with a computational time of 8.2 ms), the computational time (11 μs) of the current modeling method is notably shortened.

Meanwhile, with the addition of the bending of the third soft segment, the workspace of the current soft manipulator (500 mm in length, 520 mm in width, and 304 mm in height) is greatly enhanced compared with the previous version (260 mm in length, 240 mm in width, and 220 mm in height). Therefore, this method enhances the practical use of the manipulator for underwater grasping in the natural environment. Note that there is a tradeoff between the reduced deformation configuration space and the computational complexity. This tradeoff depends on the application backgrounds. We expect that this method will have a broader range of applications in the future: it may shed light on the modeling of other soft continuum robots that use actuation approaches other than pneumatic, such as tendon-driving manipulators, origami-structure-based manipulators, and so forth [31].

Protocols A–C

In all three scenarios, data were collected in uncontrolled sea conditions, with waves ranging from 5 to 15 cm. The experiments were conducted at an average depth of roughly 80 cm. Drag forces, depending on the wave motion and the water speed, were constantly influencing the performance of the system. Furthermore, the tests were performed only a few meters from shore, which increased the hydrodynamic disturbance. Although the pitch, roll, and yaw of the robot were somewhat affected by these disturbances, the compliance of the arm and the gripper compensated for this to some extent. Eventually, the experiments assessed the system performance in real-world conditions, which demonstrated the effectiveness of the presented solution.

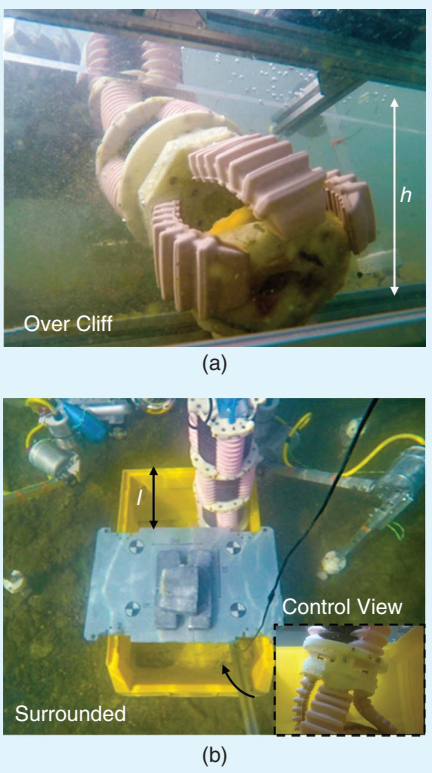

Figure 11. The results of undersea grasping in confined spaces. (a) The simulated overhang environment, where *h* is the height of the overhang. (b) The simulated enclosed environment, where *l* is the length of the opening. Scale bar: 5 cm.

The results of these protocols highlight how the robotic system was capable of exerting significant forces comparable to those obtained with an I-AUV or a small ROV but with significantly decreased power requirements. However, our benthic approach exhibits limitations related to long-range (kilometer-range) mobility. We expect benthic vehicles to complement AUV operations in small, defined areas where more accurate exploration and intervention tasks are required, while AUVs will remain the preferred choice for wide-area screening. Additionally, the soft arm benefited from operating from a stable base, and, even with real sea disturbances, effectively manipulated objects within a target area. A benthic mobile robot from which active controls can be executed seems to be a practical enhancement for UVMSs. The soft arm alone is able to exert significant force, with the qualitative advantages of grasping adaptation and high dexterity. The gripper design [32] could be improved to exploit the full potential of a pneumatic arm: a stiffness-changing solution, as presented in [33], could possibly improve both the strength and the compliance.

Protocols D–E

Tasks such as collecting objects from the sea bed require precise locomotion, arm dexterity to collect and place items, enough force to lift and free entangled objects, and a delicate touch from the gripper. The objects selected for protocol D represented a small variety of heterogeneous yet relevant categories: fragile objects, plastic litter, and solid articles. The confined spaces prepared for protocol E also represent possible man-made environments where similar tasks have to be performed. Results from these two protocols highlight the positive interaction between the legged system and the soft arm. The thruster dynamics of other systems may displace low-density target objects and damage fragile ones. With the current approach, we were able to select a slow operating speed that barely affected the environment and enabled the robot to precisely approach a target object.

In protocol D, the uncontrolled lowering motion of the legs at the end of the walking phase influenced the arm's final position, which suggests the adoption of other stopping strategies, but, in all experiments, the robot was capable of placing the object within the arm's workspace and retrieving objects from the seabed. There were some unexpected problems during the object release. We recognize that quasi-floating,

low-density objects, such as plastic bags and fishing nets, are unique articles and poorly investigated. The dexterity required to free the gripper from ensnaring objects (i.e., those that wrap around the gripper fingers) is not present in our current solution and in other grippers. We believe that, as robotic hands and grippers face increasingly complex tasks, the release problem may be the subject of further research.

Eventually, costly and dangerous tasks that human divers currently perform, such as turning valves, replacing components, and pushing buttons in confined spaces and cluttered environments, will become common applications for underwater robotic systems. However, even these apparently simple tasks are complex for underwater robots, and, to our knowledge, no attempts have been made to analyze underwater manipulation in confined environments. Our tests, although straightforward, conceptually highlight the benefit of a continuum soft arm for underwater environments. Contact with side walls did not impair the task completion, and the dexterity of the arm and gripper mostly compensated for disturbances and inaccurate positioning of the robot.

Furthermore, with the contribution of a mobile base, it was possible to retrieve objects from even very deep and narrow apertures. In constrained environments, where the arm alone was unable to exit, the robot's legs could effectively retract the arm from the aperture. Unexpected contact was damped by the passive elastic components of the arm, which helped maintain the stability of the system as a whole. A rigid solution would require computation and sensing capabilities that are often not available for underwater systems.

Conclusions

To our knowledge, this article is the first to document a synergetic robotic system composed of a benthic legged platform and soft continuum manipulator performing real-world underwater mission-like experiments. We examined the workspace extensibility, force, energy consumption, and grasping ability of the robot under different experimental scenarios. We found that the soft manipulator's workspace could be significantly extended by adding a benthic legged robot as a mobile base. The robot precisely approached and collected objects without disturbing the undersea environment, which is a common challenge for traditional screw propeller-driven ROV systems. The robot could also retrieve objects from deep apertures in overhang environments. One current limitation is that the soft manipulator and legged robot are controlled by separate systems. In the future, we aim to develop a robot with a fully integrated control system for both the soft continuum manipulation and the benthic legged locomotion.

Acknowledgments

This research was supported by the Blue Resolution Project, which is funded by Arbi Dario spa; the Chinese National Science Foundation (grants 61822303, 91848105, 61633004, and 91848206); and the National Key R&D Program of China (grants 2019YFB1309600 and 18YFB1304600).

References

[1] J. Yuh, G. Marani, and D. R. Blidberg, "Applications of marine robotic vehicles," *Intell. Serv. Robot.*, vol. 4, no. 4, pp. 221–231, 2011. doi: 10.1007/s11370-011-0096-5.

[2] "The 2018 annual report on EU blue economy," Center for Coastal & Marine Studies, Brussels, Belgium, 2018. [Online]. Available: https://op.europa.eu/en/publication-detail/-/publication/79299d10-8a35-11e8-ac6a-01aa75ed71a1

[3] G. Antonelli, *Underwater Robots, Motion and Force Control of Vehicle-Manipulator Systems* (Springer Tracts in Advanced Robotics). New York: Springer-Verlag, 2006.

[4] B. Siciliano and O. Khatib, *Springer Handbook of Robotics*. Berlin: Springer-Verlag, 2008.

[5] E. Cataldi and G. Antonelli, "Basic interaction operations for an underwater vehicle-manipulator system," in *Proc. 2015 Int. Conf. Adv. Robot.*, pp. 524–529. doi: 10.1109/ICAR.2015.7251506.

[6] E. Simetti et al., "Autonomous underwater intervention: Experimental results of the MARIS project," *IEEE J. Ocean. Eng.*, vol. 43, no. 3, pp. 620–639, 2018. doi: 10.1109/JOE.2017.2733878.

[7] R. D. Christ and R. L. Wernli, *The ROV Manual: A User's Guide to Remotely Operated Vehicles*. Amsterdam, The Netherlands: Elsevier, 2013.

[8] T. Inoue, T. Shiosawa, and K. Takagi, "Dynamic analysis of motion of crawler-type remotely operated vehicles," *Ocean. Eng. IEEE J.*, vol. 38, no. 2, pp. 375–382, 2013. doi: 10.1109/JOE.2012.2225292.

[9] Y. Kojio et al., "Walking control in water considering reaction forces from water for humanoid robots with a waterproof suit," in *Proc. IEEE Int. Conf. Intell. Robot. Syst.*, 2016, pp. 658–665. doi: 10.1109/IROS.2016.7759123.

[10] M. Ishida, D. Drotman, B. Shih, M. Hermes, M. Luhar, and M. T. Tolley, "Morphing structure for changing hydrodynamic characteristics of a soft underwater walking robot," *IEEE Robot. Autom. Lett.*, vol. 4, no. 4, pp. 4163–4169, 2019. doi: 10.1109/LRA.2019.2931263.

[11] G. Picardi, C. Laschi, and M. Calisti, "Model-based open loop control of a multigait legged underwater robot," *Mechatronics*, vol. 55, pp. 162–170, 2018. doi: 10.1016/j.mechatronics.2018.09.006.

[12] G. Picardi, S. Iacoponi, M. Chellapurath, C. Laschi, and M. Calisti, "Surveying and cleaning plastic pollution in the sediment: SILVER+ approach," in *Proc. Oceans 2019*, pp. 1–8. doi: 10.1109/OCEANSE.2019.8867331.

[13] I. Vasilescu et al., "AMOUR V: A hovering energy efficient underwater robot capable of dynamic payloads," *Int. J. Robot. Res.*, vol. 29, no. 5, pp. 547–570, 2010.

[14] C. Laschi, B. Mazzolai, M. Cianchetti, L. Margheri, M. Follador, and P. Dario, "Soft robot arm inspired by the octopus," *Adv. Robot.*, vol. 26, no. 7, pp. 709–727, 2012. doi: 10.1163/156855312X626343.

[15] D. M. Lane et al., "AMADEUS: Advanced manipulation for deep underwater sampling," *IEEE Robot. Autom. Mag.*, vol. 4, no. 4, pp. 34–45, 1997. doi: 10.1109/100.637804.

[16] F. Renda, M. Cianchetti, M. Giorelli, A. Arienti, and C. Laschi, "A 3D steady-state model of a tendon-driven continuum soft manipulator inspired by the octopus arm," *Bioinspir. Biomime.*, vol. 7, no. 2, p. 025006, 2012. doi: 10.1088/1748-3182/7/2/025006.

[17] M. Calisti et al., "Design and development of a soft robot with crawling and grasping capabilities," in *Proc. IEEE Int. Conf. Robot. Autom.*, 2012, pp. 4950–4955. doi: 10.1109/ICRA.2012.6224671.

[18] K. C. Galloway et al., "Soft robotic grippers for biological sampling on deep reefs," *Soft Robot.*, vol. 3, no. 1, pp. 23–33, 2016. doi: 10.1089/soro.2015.0019.

[19] S. Kurumaya et al., "A modular soft robotic wrist for underwater manipulation," *Soft Robot.*, vol. 5, no. 4, pp. 399–409, 2018. doi: 10.1089/soro.2017.0097.

[20] B. T. Phillips et al., "A dexterous, glove-based teleoperable low-power soft robotic arm for delicate deep-sea biological exploration," *Sci. Rep.*, vol. 8, p. 14,779, Oct. 2018. doi: 10.1038/s41598-018-33138-y.

[21] S. Licht, E. Collins, M. L. Mendes, and C. Baxter, "Stronger at depth: Jamming grippers as deep sea sampling tools," *Soft Robot.*, vol. 4, no. 4, pp. 305–316. 2017. doi: 10.1089/soro.2017.0028.

[22] G. Picardi, M. Chellapurath, S. Iacoponi, S. Stefanni, C. Laschi, and M. Calisti, "Bioinspired underwater legged robot for seabed exploration with low environmental disturbance," *Sci. Robot.*, vol. 5, no. 42, 2020. [Online]. Available: https://robotics.sciencemag.org/content/5/42/eaaz1012.full.pdf, doi: 10.1126/scirobotics.aaz1012.

[23] A. Parmiggiani, G. Metta, and N. Tsagarakis, "The mechatronic design of the new legs of the iCub robot," in *Proc. IEEE-RAS Int. Conf. Human. Robots*, 2012, pp. 481–486. doi: 10.1109/HUMANOIDS.2012.6651563.

[24] M. Calisti and C. Laschi, "Underwater running on uneven terrain," in *Proc. OCEANS 2015-Genova*, pp. 1–5. doi: 10.1109/OCEANS-Genova.2015.7271366.

[25] J. Burgner-Kahrs, H. B. Gilbert, J. Granna, P. J. Swaney, and R. J. Webster, "Workspace characterization for concentric tube continuum robots," in *Proc. IEEE Int. Conf. Intell. Robots Syst.*, 2014, pp. 1269–1275. doi: 10.1109/IROS.2014.6942720.

[26] B. A. Jones, W. McMahan, and I. D. Walker, "Practical kinematics for real-time implementation of continuum robots," in *Proc. IEEE Int. Conf. Robot. Autom.*, 2006, pp. 1840–1847. doi: 10.1109/ROBOT.2006.1641974.

[27] T. George Thuruthel, Y. Ansari, E. Falotico, and C. Laschi, "Control strategies for soft robotic manipulators: A survey," *Soft Robot.*, vol. 5, no. 2, pp. 149–163, 2018. doi: 10.1089/soro.2017.0007.

[28] Z. Gong et al., "A soft manipulator for efficient delicate grasping in shallow water: Modeling, control, and real-world experiments," *Int. J. Robot. Res.*, 2020. [Online]. Available: https://doi.org/10.1177/0278364920917203, doi: 10.1177/0278364920917203.

[29] J. G. Bellingham et al., "Efficient propulsion for the tethys long-range autonomous underwater vehicle," in *Proc. 2010 IEEE/OES Auton. Underwater Veh.*, pp. 1–7. doi: 10.1109/AUV.2010.5779645.

[30] B. O. A. Haugaløkken, E. K. Jørgensen, and I. Schjølberg, "Experimental validation of end-effector stabilization for underwater vehicle-manipulator systems in subsea operations," *Robot. Auton. Syst.*, vol. 109, pp. 1–12, Nov. 2018. doi: 10.1016/j.robot.2018.08.007.

[31] L. Wen, F. Pan, and X. Ding, "Tensegrity metamaterials for soft robotics," *Sci. Robot.*, vol. 5, no. 45, p. eabd9158, Aug. 2020. doi: 10.1126/scirobotics.abd9158.

[32] Y. Hao et al., "Modeling and experiments of a soft robotic gripper in amphibious environments," *Int. J. Adv. Robot. Syst*, vol. 14, no. 3, 2017. doi: 10.1177/1729881417707148.

[33] H. Stuart, S. Wang, O. Khatib, and M. R. Cutkosky, "The Ocean One hands: An adaptive design for robust marine manipulation," *Int. J. Robot. Res.*, vol. 36, no. 2, pp. 150–166, 2017. doi: 10.1177/0278364917694723.

Jiaqi Liu, School of Mechanical Engineering and Automation, Beihang University, Beijing. Email: jiaqiliu@buaa.edu.cn.

Saverio Iacoponi, BioRobotics Institute and Department of Excellence in Robotics and AI, Scuola Superiore Sant'Anna, Pisa, Italy. Email: saverio.iacoponi@santannapisa.it.

Cecilia Laschi, BioRobotics Institute and Department of Excellence in Robotics and AI, Scuola Superiore Sant'Anna, Pisa, Italy. Email: cecilia.laschi@santannapisa.it.

Li Wen, School of Mechanical Engineering and Automation, Beihang University, Beijing. Email: liwen@buaa.edu.cn.

Marcello Calisti, BioRobotics Institute and Department of Excellence in Robotics and AI, Scuola Superiore Sant'Anna, Pisa, Italy. Email: marcello.calisti@santannapisa.it.